Dynamics of laser ablation plume penetration through low pressure background gases

David B. Geohegan
Solid State Division, Oak Ridge National Laboratory, Oak Ridge, Tennessee 37831-6056

Alexander A. Puretzky
Institute of Spectroscopy, Russian Academy of Sciences, Troitsk, Russia

The dynamics of laser-ablated yttrium plume propagation through background argon have been investigated with fast time- and spatially-resolved plasma diagnostics in order to characterize a general phenomenon believed to be important to film growth by pulsed laser deposition (PLD). During expansion into low-pressure background gases, the ion flux in the laser ablation plasma plume is observed to split into fast and slow components over a limited range of distances including those typically utilized for PLD. Optical absorption and emission spectroscopy are employed to simultaneously identify populations of both excited and ground states of Y and Y^+. These are correlated with intensified-CCD (ICCD) photographs of visible plume luminescence and ion fluxes recorded with fast ion probes. These measurements indicate that plume-splitting in background gases is consistent with scattering of target constituents by ambient gas atoms. The momentum transfer from these collisions produces a transition from the initial, "vacuum" velocity distribution into a velocity distribution which is significantly slowed in accordance with shock or drag propagation models. © *1995 American Institute of Physics.*

The slowing and attenuation dynamics of laser ablation plasmas in low-pressure background gases are of significant interest for film growth by pulsed-laser deposition (PLD) since the magnitude and kinetic energy of the species arriving at the substrate are key processing parameters.[1,2] Reported here are combined diagnostic measurements of ablation plume penetration through background gases during a key transitional regime in which the ion flux is split into distinct fast and slowed components. This apparently general phenomenon occurs over a limited range of distances at ambient pressures, including those typically used for PLD (as reported for YBCO ablation into O_2).[2–5] This "plume-splitting" is significant because a "fast" component of ions can arrive at the ion probe (or substrate) with little or no delay compared to propagation in vacuum (i.e., Y^+ kinetic energies in this study were up to 250 eV). However, at longer distances this fast component is completely attenuated, and a single, slowed distribution of ions is observed. This fast component is easily overlooked in imaging studies because enhanced plume luminescence occurs in the slowed distribution.

Fast ion probes provide convenient measurements of the magnitude and time-of-flight of the ion current (flux) in plasma plumes propagating through background gases. Exponential losses in the ion flux are induced by the background gas as the propagation distance or ambient density are increased, in general agreement with a simple scattering model (effective cross sections $\sim 1 \times 10^{-16}$ cm^2).[2–4,6] Eventually, ion probe and fast imaging measurements record a decelerating, stable shock-structure which propagates in accordance with drag or shock models.[4–7] Although these models adequately describe the propagation of the "slow" component, the fast distribution can be interpreted[2–4] as ions which have penetrated the background gas without significant collisions, and are statistically attenuated with distance.

Recent Monte Carlo simulations have successfully simulated such a fast transmitted flux through a background gas.[8] However, several alternative gas-dynamic and scattering explanations can be imagined to describe the two components, including ionization and snowplowing of the background gas[9–11] or species-dependent scattering.

In this letter, time- and spatially-resolved optical absorption and emission spectroscopy are applied to determine the composition of the fast and slow propagating plume components for single-component target ablation (yttrium) into an inert gas (argon) and are correlated with quantitative imaging and ion probe measurements. Although the splitting effect appears quite general, the yttrium/argon system was chosen because optical absorption spectroscopy of both Y and Y^+ was simultaneously possible[12] and argon is chemically inert.

The experimental apparatus has been described previously.[3–7,12] A cylindrical lens ($f_L = 500$ mm) focused the apertured 248 nm beam from a Questek 2960 KrF-excimer laser (28 ns FWHM pulse width) to a horizontal line (2.0 cm×0.075 cm) on the face of a sanded yttrium (99.99%) pellet at an incidence angle of 30°. For optical absorption spectroscopy, a pulsed (1.5 μs FWHM) Xe lamp beam (width 0.5 mm) was passed parallel to the target surface and just above a wire ion probe tip (floating bias −70 V with respect to its shield). The expansion of the ablated yttrium formed a vertical fan which expanded little along the horizontal lamp beam axis (toward the camera or spectrometer), so the absorption path length remained at approximately 2 cm for the two distances investigated here $d=1.5, 2.5$ cm). Optical detection utilized a 1.33 m spectrometer (McPherson 209, 1800 g/mm holographic grating) outfitted with an intensified, gated diode array (Princeton Instruments IRY-700RB, 5 ns resolution) and photomultiplier tube (Hamamatsu R955). Fast unfiltered imaging was performed with a gated, (ICCD), lens-coupled camera system (Princeton Instruments)
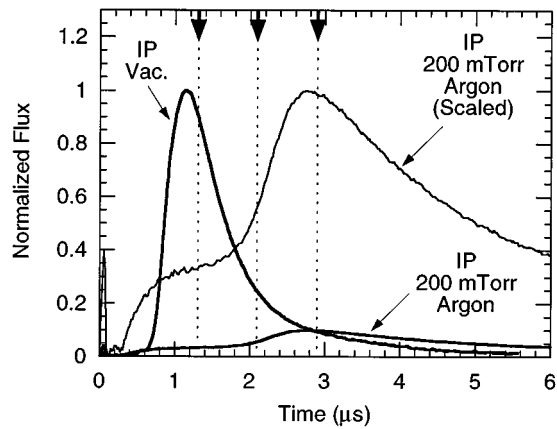
FIG. 1. Ion probe current pulses measured $d=1.5$ cm along the normal to a yttrium target following KrF-laser irradiation (0.8 J/cm^2) in vacuum (1 $\times 10^{-6}$ Torr) and in 200 mTorr argon. The bimodal 200 mTorr wave form is plotted in correct magnitude relative to the vacuum pulse and also is replotted scaled up by a factor of 10. (Note the actual magnitude of the fastest material, which is attributed to Y^{++}.) The peak of the vacuum pulse corresponds to a current flux of 25 A/cm^2. Three times are marked by arrows for comparison with the imaging and optical absorption measurements of Fig. 3.

FIG. 3. Time-resolved optical absorption spectra [$\log_{10}(I_0/I)$] of ground-state Y, Y$^+$ [(a)–(c); into the page at $d=1.5$ cm, 200 ns gates] and ICCD photographs of the visible plasma luminescence [(d)–(i); 50 ns gates] at 1.3, 2.1, and 2.9 μs following KrF-laser irradiation of yttrium into 200 mTorr argon (see arrows indicating times in Fig. 1). Y$^+$ ion lines dominate absorption at (c) 1.3 μs and (b) 2.1 μs (first peak, shoulder of ion probe signal): 358.45, 360.07, 360.19, 361.10, 362.87, 363.31 nm. Y neutral absorption becomes noticeable in the second peak of the ion probe signal as indicated in (a) 2.9 μs, at 359.29, 362.09 nm. For (d)–(i), equal exposures were used; each image is plotted twice [image data normalized to (d) 10 000, (e) 20 000, (f)–(i) 38 000 counts].

with variable gain, 200–820 nm response, and variable gating above 5 ns.

A comparison of digitized ion probe currents in vacuum and in 200 mTorr argon is presented in Fig. 1. Although the ion flux is greatly attenuated, two dominant distributions of ions are observed in argon at $d=1.5$ cm: A component apparently penetrating the background gas with nearly the same velocities as in vacuum, and the other component peaking much later in time. This interpretation was tested by additional fast imaging and absorption spectroscopy measurements carried out at the times indicated (see arrows) in Fig. 1.

Fast images of the visible plume luminescence in vacuum and in 200 mTorr argon are given in Fig. 2 at Δt $=0.60$–0.65 μs following the laser pulse. The formation of a bright peak in the emission, indicative of a shock structure, is clearly evident in the body of the plume in argon [Fig. 2(b)]. In order to correctly judge the maximum extent of the 200 mTorr emission relative to vacuum, a 10 grayscale palette of equal normalization is applied to the same images and replotted as Figs. 2(c) and 2(d). Although this sacrifices details of

the bright shock structure, it clearly reveals that material has penetrated ahead of the bright shock front in 200 mTorr argon, to distances comparable to those in vacuum. Figure 2(e) gives a line profile of the emission intensity from the irradiated spot along the target normal. The emitted light intensity in argon exceeds the vacuum intensity at long distances from the target, while close to the target the emission intensities are remarkably similar.

Similar pairs of fast images of the visible plume luminescence at 1.3, 2.1, and 2.9 μs are presented in Figs. 3(d)–3(i) for correlation with the first peak, shoulder, and second peak of the 200 mTorr ion probe current of Fig. 1. In addition, to investigate the populations of ground-state Y and Y$^+$ at the same three times, gated optical absorption spectra (200 ns width, 100 spectra averaged) are given in Figs. 3(a)–3(c) for the region just above the wire ion probe tip at $d=1.5$ cm.
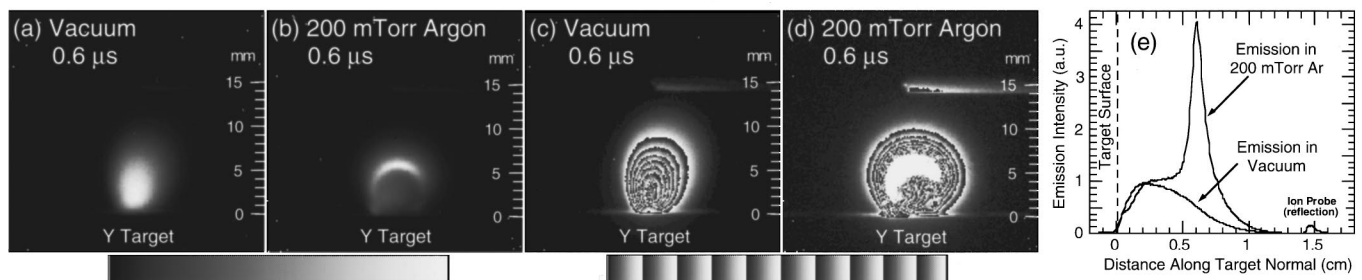

FIG. 2. Gated ICCD photographs of the total visible optical plasma emission intensity at $\Delta t=0.60$–0.65 μs following KrF-laser irradiation (0.8 J/cm^2) of yttrium metal into (a), (c) 1×10^{-6} Torr and (b), (d) 200 mTorr argon. The single-grayscale palette is normalized to (a) 8100 counts and (b) 34000 counts. The same photographs are replotted with a 10 grayscale palette (equal normalization to 10000 counts) in (c) and (d). A line profile of the emission intensity along the target normal (e) shows the correct relative scaling between the vacuum and background images. The wire ion probe is visible at $d=1.5$ cm.
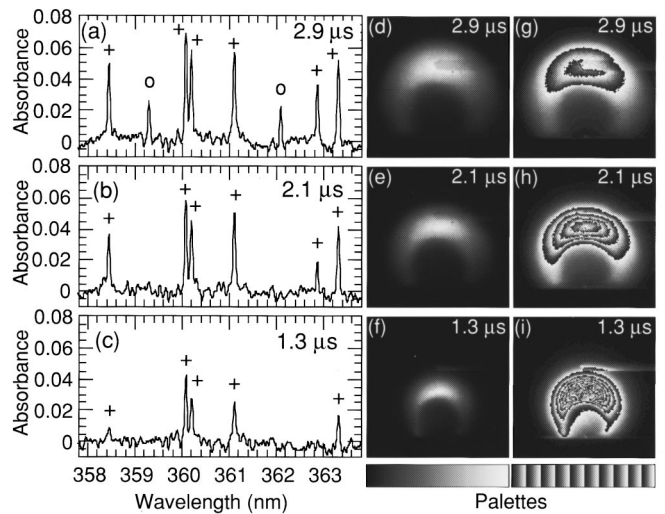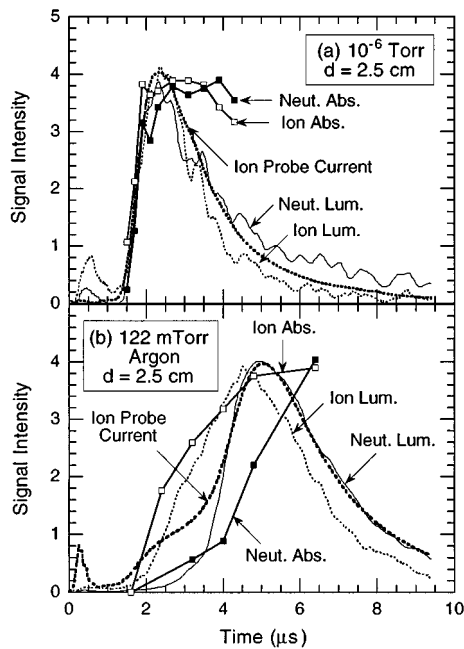
    D. B. Geohegan and A. A. Puretzky

FIG. 4. Normalized ion probe current (IP), luminescence (lum) intensities of Y*(410.2 nm) and Y$^+$*(363.3 nm), and optical absorbances (absc.) of Y(362.1 nm) and Y$^+$(363.3 nm) at d=2.5 cm following 0.8 J/cm^2 KrF-laser irradiation of yttrium in (a) vacuum (1×10^{-6} Torr) and (b) 122 mTorr argon. Scaling factors: (a) lum: Y*(/3), Y$^+$* (×1), absc: Y(×70), Y$^+$(×94), IP(mV/81), (b) lum: Y*(/23), Y$^+$*(/12.5), absc: Y(×100), Y$^+$(×70), IP(mV/81).

At 1.3 μs [Fig. 3(f) and 3(i)], very weak optical emission is present at the probe position during the first peak of the ion flux signal. However, the optical absorption spectrum [Fig. 3(c)] reveals strong Y$^+$ absorption [lines indicated by + in Figs. 3(a)–3(c)] at this time, confirming the penetration of target ions through the background gas at "vacuum" velocities. At 2.1 μs [Figs. 3(e) and 3(h)] the steep gradient of plume luminescence has reached the probe at 1.5 cm (shoulder of the ion probe current, Fig. 1). The peak luminescence is 1.9 times smaller than at 1.3 μs, and the optical absorption spectrum is still dominated by Y$^+$ absorption. During the second peak of the ion probe current at 2.9 μs, the probe is immersed in the brightest region of luminescence [Figs. 3(d) and 3(g)] which is half the peak intensity of that at 2.1 μs. In addition to the ion lines, ground-state neutral yttrium becomes noticeable [lines indicated by ○ in Fig. 3(a)].

At longer distances, a similar situation exists at lower pressures. Figure 4 shows a comparison of ion probe current, optical emission intensity (of Y* and Y$^+$*), and optical absorbance (of Y and Y$^+$) time dependences at d=2.5 cm following KrF-laser irradiation of yttrium in (a) vacuum (1 $\times 10^{-6}$ Torr) and (b) 122 mTorr argon. In vacuum [Fig. 4(a)], ground-state neutrals and ions are found (through optical absorption) in coincidence with excited ions and neutrals (from optical emission) on the leading edge of the ion probe current. In background argon [Fig. 4(b)], excited and ground-state Y$^+$ ions dominate the first peak of the ion probe wave form, while excited and ground-state neutrals appear in the delayed, second distribution.

In summary, simultaneous application of the four diagnostic techniques confirms that a component of target material is transmitted through low-pressure background gases with little or no delay compared to vacuum. Weak optical emission from this fast component originates principally from yttrium ions. Ground state and excited neutrals, which are present during the fast vacuum distribution, appear delayed (or depopulated) at similar times in background gases and are correlated principally with the bright luminescence at the slowed, second peak of the ion probe signal.

The data are consistent with scattering over extended distances in which ions and atoms in the ablation plume undergo collisions with mean-free-paths ~1 cm at 200 mTorr. Plume material is retarded from the fast vacuum velocity distribution due to momentum transfer with the background gas (as well as other retarded plume material). This slowed material becomes observable as a distinct second distribution only for a limited range of distances and pressures.

The luminescence represents populations of short-lived excited states (radiative lifetimes ~10 ns) which can be populated by a variety of collisional processes, including three-body recombination of ions with electrons, electron-impact excitation of ground and low-lying states of neutrals and ions, and collisional or radiative deactivation of Rydberg states. The luminescence intensity does not necessarily correspond to the overall plume density, but is determined by velocity- or temperature-dependent rate constants and their effects on the population kinetics of luminescent levels. The enhanced luminescence in the slowed "shock region" is explained generally by favorable population kinetics there. The depletion of ground- and excited-state neutrals observed in the fast distribution is more likely the result of conversion to neutral Rydberg states or ions than a preferential slowing of neutrals. A detailed experimental description of the plume luminescence and implications for plume temperatures and density redistributions, as well as computer simulation of the above effects, will be presented elsewhere.

[1] R. Kelly and A. Miotello, in *Pulsed Laser Deposition of Thin Films,* edited by D. B. Chrisey and G. K. Hubler (Wiley, New York, 1994), Chap. 3 and references cited therein.
[2] D. B. Geohegan in Ref. 1, Chap. 5.
[3] D. B. Geohegan, in *Laser Ablation: Mechanisms and Applications,* edited by J. C. Miller and R. F. Haglund (Springer, Heidelberg, 1991), p. 28.
[4] D. B. Geohegan, Thin Solid Films **220**, 138 (1992).
[5] D. B. Geohegan, in *Laser Ablation of Electronic Materials: Basic Mechanisms and Applications,* edited by E. Fogarassy and S. Lazare (North Holland, Amsterdam, 1992), p. 73.
[6] D. B. Geohegan, in *Excimer Lasers*, NATO ASI Series E: Applied Sciences Vol. 265, edited by L. D. Laude (Kluwer, Netherlands, 1994).
[7] D. B. Geohegan, Appl. Phys. Lett. **60**, 2732 (1992).
[8] J. C. S. Kools, J. Appl. Phys. **74**, 6401 (1993).
[9] R. R. Goforth and D. W. Koopman, Phys. Fluids **17**, 698 (1974).
[10] David W. Koopman and R. R. Goforth, Phys. Fluids **17**, 1560 (1974).
[11] David W. Koopman, Phys. Fluids **15**, 1959 (1972).
[12] D. B. Geohegan and D. N. Mashburn, Appl. Phys. Lett. **55**, 2345 (1989).